Journal of Magnetism and Magnetic Materials 380 (2015) 111–116

Contents lists available at ScienceDirect

Journal of Magnetism and Magnetic Materials

journal homepage: www.elsevier.com/locate/jmmm

Mössbauer, magnetization and X-ray diffraction characterization methods for iron oxide nanoparticles

Raul Gabbasov [a,*], Michael Polikarpov [a], Valery Cherepanov [a], Michael Chuev [b], Iliya Mischenko [b], Andrey Lomov [b], Andrew Wang [c], Vladislav Panchenko [a]

[a] National Research Center "Kurchatov Institute", Moscow, Russia
[b] Institute of Physics and Technology, Russian Academy of Sciences, Moscow, Russia
[c] Ocean NanoTech. Springdale, AR, USA

ARTICLE INFO

Article history:
Received 30 June 2014
Received in revised form
29 October 2014
Accepted 2 November 2014
Available online 13 November 2014

Keywords:
Iron oxide nanoparticles
Mössbauer spectroscopy
X-ray diffraction
Ferrimagnetism

ABSTRACT

Water soluble magnetite iron oxide nanoparticles with oleic polymer coating and average diameters in the range of 5–25 nm, previously determined by TEM, were characterized using Mössbauer, magnetization and X-ray diffraction measurements. Comparative analysis of the results demonstrated a large diversity of magnetic relaxation regimes. Analysis showed the presence of an additional impurity component in the 25 nm nanoparticles, with principally different magnetic nature at the magnetite core. In some cases, X-ray diffraction measurements were unable to estimate the size of the magnetic core and Mössbauer data were necessary for the correct interpretation of the experimental results.

1. Introduction

Iron oxide nanoparticles based on magnetite Fe_3O_4 and maghemite γ-Fe_2O_3 have long attracted the attention of researchers due to their advanced magnetic properties. Because of their biocompatibility and biodegradability [1–3], iron oxide nanoparticles are considered to be key components of invasive medical procedures such as targeted drug delivery and hyperthermia [4–7]. The effectivity of these applications strongly depends on the magnetic dynamics of nanoparticles, which is related to the relaxation rates of nanoparticle magnetization vectors as determined by the size of nanoparticles. There are a number of methods to determine the size of nanoparticles including transmission electron microscopy (TEM), X-ray diffraction, magnetic measurements, hydrodynamic methods and light scattering. The size of the nanoparticle determined by one method depends on the nanoparticle's quantum mechanical and magnetic properties and can be different from the size determined by other methods. None these methods, except magnetic measurements, is able to provide reliable information about nanoparticle magnetic properties and dipole interactions.

In the vast majority of nanoparticle ensembles, interparticle magnetic dipole interaction between single nanoparticles takes place. Consequently, the relaxation of the magnetization vector of individual nanoparticles cannot be considered separately from the whole ensemble. The magnetization vectors of neighboring nanoparticles influence each other and slow down relaxation processes in comparison to non-interacting particles under the same physical conditions. As a result, the physical size of individual nanoparticles may have little connection to the magnetic dynamics of the ensemble. This lack of connection usually takes place for nanoparticles administered to a live organism. In this in vivo case, the dipole interaction between nanoparticles is weaker in comparison to the samples measured in vitro [8]. In fact, in the ensemble of interacting nanoparticles, there is a relaxation of the magnetization vector of the cluster of nanoparticles bounded with each other by magnetic dipole interaction. The size of the cluster determines the relaxation rate in the nanoparticle ensemble according to the Néel's formula:

$$p = p_0 \exp(-KV/k_BT) \quad (1)$$

where p_0 is the fluctuation rate slightly dependent on temperature T, V is the particle's volume, k_B is the Boltzmann constant and K-anisotropy energy density. In this formula, the information about cluster size is contained in Néel's barrier height KV. Consequently, it may be convenient to use the value of Néel's barrier height for parameterization of the cluster size [9,10]. A method capable of estimating cluster size must be sensitive to changes of the magnetic field at frequencies comparable to the oscillation rates of the magnetization vectors in the ensemble.

* Corresponding author.
E-mail address: gabbasov-raul@yandex.ru (R. Gabbasov).

http://dx.doi.org/10.1016/j.jmmm.2014.11.032
0304-8853/

One of the most reliable methods for the investigation of nanoparticle magnetic dynamics is gamma-resonance (Mössbauer) relaxation spectroscopy. This method has demonstrated unique possibilities for *in vivo* investigations in which it was necessary to obtain quantitative information in the presence of endogenous iron not connected to injected nanoparticles [1–3,8]. Mössbauer spectroscopy considers a group of nanoparticles as a cluster of interacting single domain magnetic particles and gives information about magnetic interactions which is essential for applications involving a magnetic field such as targeted drug delivery. Magnetic dipole interactions can have a significant influence on magnetic dynamics resulting in magnetically split Mössbauer spectra with asymmetrically broadened sextets, while non-interacting particles show a quadrupole doublet because of fast superparamagnetic relaxation [9,10].

The Mössbauer spectrum depends strongly on nanoparticle size (in the case of interacting nanoparticles – the cluster size). For small nanoparticles, the relaxation rate of their magnetization vector becomes much faster than the Larmor frequency of the nuclear spin precession. As a result, the mean value of hyperfine becomes zero and their Mössbauer spectra demonstrate quadrupole doublet or singlet. In the case of large nanoparticles, when the nanoparticle magnetization vector saves its direction during the Larmor precession time, a well-resolved static hyperfine magnetic structure with the Zeeman sextet of lines appears in the spectrum. The reverse process occurs when the measurement temperature increases. The Mössbauer spectrum of the superparamagnetic particles changes with increasing temperature from a Zeeman sextet to a paramagnetic doublet (or singlet). The interpretation of Mössbauer spectra is determined by applying a theoretical model. Iron oxide nanoparticles, which are large and have inverse spinel structure and intermediate stoichiometry between magnetite and maghemite, usually demonstrate ferrimagnetic behavior. Their Mössbauer spectra contain two or more well-resolved sextet components related to nonequivalent magnetic sublattices with different spin characteristics. However, when the applied magnetic field is strong enough, the magnetization vectors of these sublattices align along, or near, the applied field direction [11]. In the Mössbauer spectrum, the spectral components of each sublattice become almost indistinguishable and the sample can be treated as ferromagnetic.

According to the core–shell model [12–14], with nanoparticle size increasing, a gradual growth of ferrous component takes place as part of magnetite (so-called “core”) versus the “shell”, ferric iron, usually attributed to maghemite. In this case, the Mössbauer spectrum demonstrates a gradual increasing of the average isomer shift [15] and the difference between the “core” and “shell” components becomes more significant. In the present study, the size effects for the set of nanoparticles were investigated by Mössbauer spectroscopy, X-ray diffraction and TEM methods.

2. Materials and methods

2.1. Preparation

We used iron oxide nanoparticles synthesized by Ocean Nanotech [16] according to the method described in [17,18]. Iron oxide powder was dissolved by oleic acid upon heating to about 200 °C, resulting in an iron oleate complex. This complex was unstable at temperatures above 250 °C. Black magnetite nanoparticles were formed above 300 °C. After the procedure, the reaction mixture was cooled and the nanoparticles were precipitated by adding chloroform and acetone. The size of the nanoparticles was controlled by the reaction time, temperature, and iron oxide and oleic acid concentrations. Their organic shells consisted of a layer of oleic acid. The mean sizes of nanoparticles were estimated using TEM and were approximately equal to 5, 10, 15, 20 and 25 nm (samples S5, S10, S15, S20 and S25), respectively (Fig. 1).

2.2. X-ray diffraction

X-ray diffraction measurements were carried out on a Rigaku Smartlab diffractometer using the planar monochromator method and Cu Kα radiation. The samples were placed on a silicon holder. XRD data were collected in the range of 20–80°. Calculation of the cell parameters was performed using the Voigt Profile fitting procedure described in [19]. The average crystalline size of the diffraction line widths was estimated using the Scherrer formula. In the calculation procedure, the line widths of the most intensive peak were used (440).

2.3. Magnetization

The magnetization measurements of the samples were performed using the Quantum Design Vibrating Sample Magnetometer with oscillation frequency 40 Hz. Hysteresis loops were measured at the temperature 300 K with magnetic field amplitude 1 kOe and constant step 25 Oe. All samples were placed in gelatin capsules.

2.4. Mössbauer spectroscopy

Mössbauer spectra were measured using the spectrometer MS-1104Em, working in the constant acceleration mode. 57Co (Rh) was used as a source of gamma-radiation. Isomer shifts were determined in relation to the centroid of α-Fe. The samples were measured at the temperatures 77 and 300 K and in the presence of a magnetic field of 3.4 kOe at 300 K.

3. Results

The TEM images of the samples S5–S25 are shown in Fig. 1. All samples demonstrate well-defined sharp size distribution and a significant extent of aggregation, which points to the presence of magnetic dipole interactions.

All X-Ray diffraction patterns contain a reference line (200) with various amplitudes which related to the silicon holder (Fig. 1). The X-ray diffraction peaks for all samples correspond to the inverse-spinel structure (Fe_3O_4). The diffraction pattern of the sample S5 has extremely broad line widths because of its small size. Nevertheless, there are still-detectable peaks located on the same diffraction angles as in other samples. The ratios of peak intensities for S10–S20 are roughly equal, which points to a similar phase composition. However the peak (400) for S25 is significantly more intense than the ones for other samples, which suggests the presence of an additional phase in this sample. The average crystalline sizes d_{XRD} obtained from the diffractions pattern (Table 1) are comparable with the mean diameters, d_{TEM}, evaluated from TEM images. However, d_{XRD} for the S25 sample is less than d_{XRD} for S20. This discrepancy can be associated with the presence in the sample S25 of additional disordered layer preventing coherent X-rays scattering.

The magnetization curves S10–S20 demonstrate typical superparamagnetic behavior. S5 is practically paramagnetic with its magnetization curve differing only slightly from a straight line (Fig. 2). No curves have any sign of a hysteresis loop at room temperature. The S25 curve demonstrates untypical behavior. At low fields (up to 500 Oe), the magnetization curve of the S20 sample surpasses the magnetization curve of the S25 sample. Above 500 Oe, the opposite occurs: the S25 curve's growth rate

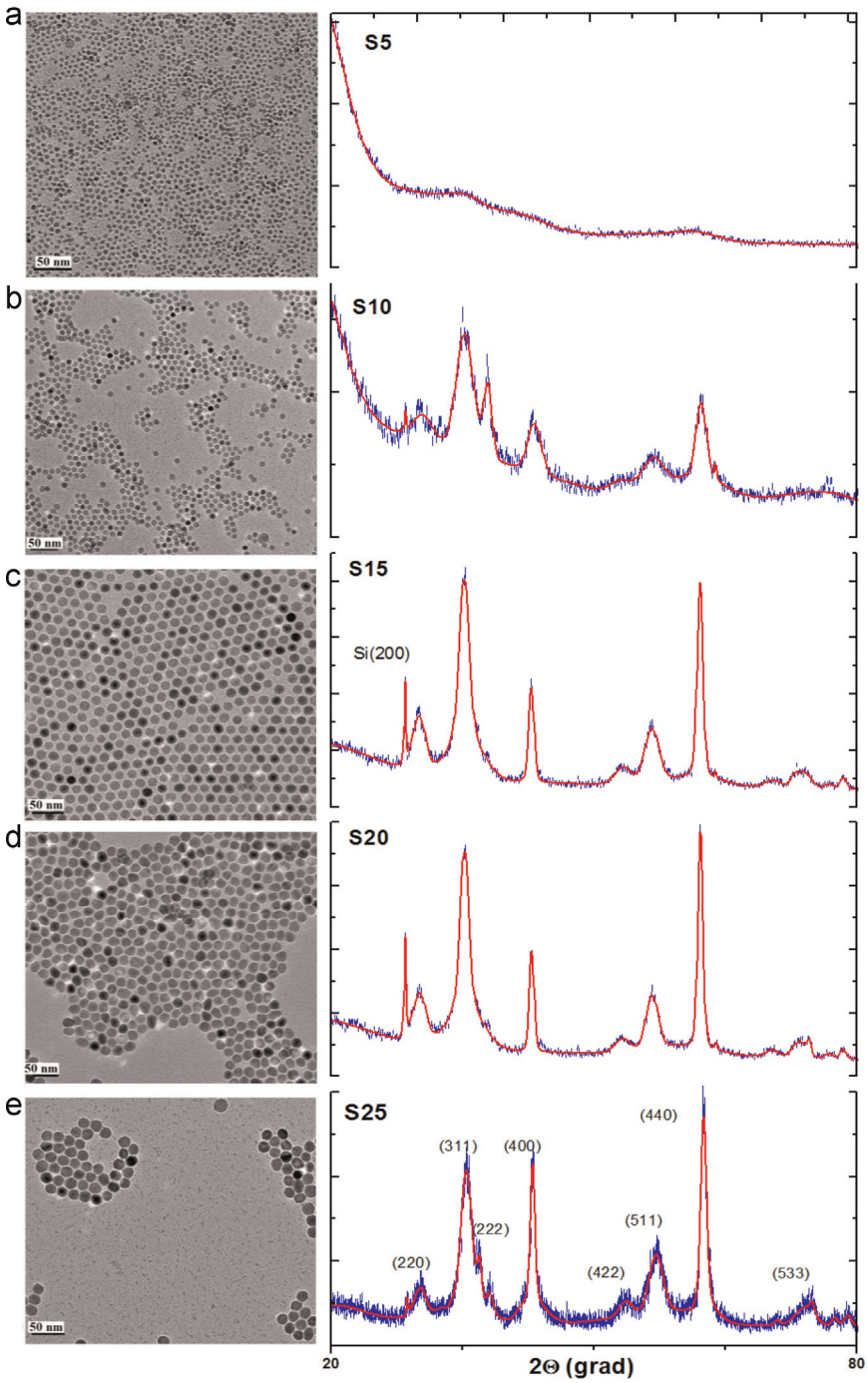

Fig. 1. (a)–(e) TEM images [16] and XRD pattern of the S5, S10, S15, S20, and S25 samples respectively.

becomes considerably faster than that of the S20 one. Such deviation from usual superparamagnetic behavior points to the presence of an additional component whose contribution is negligible at low fields and becomes significant at high fields.

The set of Mössbauer spectra is shown in Fig. 4. The 300 K spectrum for S25 contains an intense singlet which restores the six-line structure at 78 K. This singlet has an unusually high isomer shift of about 1.1 mm/s. The other samples do not show any sign of a component with such a high isomer shift. Such an isomer shift can be attributed to an additional component corresponding to ferrous iron.

The Mössbauer spectra of S10–S25 at temperatures 78 K and 300 K (Fig. 3a, b) were fitted with good precision using the ferrimagnetic model of magnetic relaxation [20]. The spectral parameters obtained are shown in Table 1. The principally different line shapes of the 78 K and 300 K spectra for S10 should be noted. At 78 K the spectrum demonstrates hyperfine structure consisting of two six-line components (A and B components). However, at 300 K these components collapse to broad doublets due to increasing relaxation rate. But even at 78 K, the spectrum contains a doublet related to the fraction of small nanoparticles.

The spectra of the S5 sample demonstrate their principle difference in shape when compared to the other samples. At a temperature of 300 K, the line width becomes broader than at 78 K, in contrast to conventional relaxation spectra. The isomer shifts in the spectra correspond to iron atoms in γ-Fe_2O_3, however the anomalous line broadening can be related to the specific energy spectrum of antiferromagnetic particles with four excitation

Table 1
Parameters of the S5–S25 samples obtained from TEM, XRD and temperature Mössbauer measurements. KV-Neel's barrier height, q_A, q_B, $H_{hf\ A}$, $H_{hf\ B}$, δ_A, δ_B-quadrupole splitting, hyperfine field and isomer shift of A and B components respectively.

Sample	**S5**		**S10**		**S15**		**S20**		**S25**	
d_{TEM}, nm	5		10		15		20		25	
d_{XRD}, nm	2.9(2)		14 (1)		22 (1)		27 (1)		24 (1)	
***T*, K**	**78**	**300**	**78**	**300**	**78**	**300**	**78**	**300**	**78**	**300**
Sextet components										
KV, K	206 (4)		209 (2)	200 (40)	770 (20)	150 (10)	750 (20)	736 (3)	390 (40)	540 (30)
q_A, mm/s	0.346 (2)		0.34 (1)	0.37 (1)	0.23 (1)	0.35 (5)	0.19 (1)	0.35 (1)	0.17 (1)	0.35 (2)
q_B, mm/s			0.27 (3)	0.40 (3)	0.20 (2)	0.35 (7)	0.05 (5)	0.35 (1)	0.35 (2)	0.35 (4)
$H_{hf\ A}$, kOe	300 (5)	275 (6)	490 (1)	500 (50)	513 (1)	500 (5)	520 (1)	469 (1)	512 (1)	478 (1)
$H_{hf\ B}$, kOe			494 (1)	500 (50)	516 (1)	350 (5)	526 (1)	410 (1)	512 (1)	499 (2)
δ_A, mm/s	0.45 (1)	0.35 (6)	0.31 (1)	0.31 (1)	0.36 (1)	0.39 (1)	0.36 (1)	0.36 (1)	0.39 (1)	0.63 (1)
δ_B, mm/s			0.74 (1)	0.43 (3)	0.67 (1)	0.38 (1)	0.62 (1)	0.36 (1)	0.79 (1)	0.14 (2)
Doublet components										
$2q_d$, mm/s			0		0.52 (3)		0.43 (5)		0.48 (2)	0
δ_d, mm/s			0.41 (1)		0.1 (1)		0.11 (3)		0.13 (1)	1.19 (1)

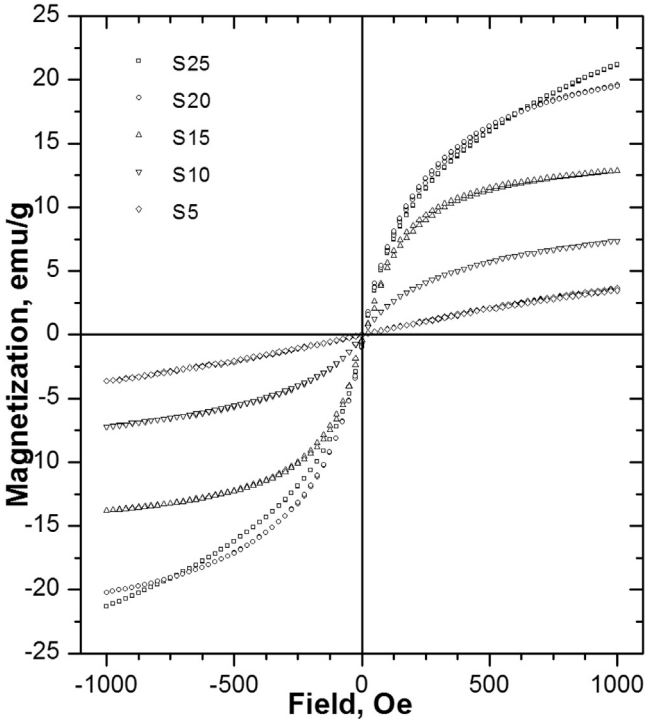

Fig. 2. Field dependent magnetization of the S5–S25 samples measured at 300 K.

branches [21]. These spectra are fitted by one broadened doublet. None of the three spectra show any sign of additional components.

The Mössbauer spectra of S10–S25 in a magnetic field (Fig. 3c) used the ferromagnetic model of magnetic relaxation [11]. The main parameters are shown in Table 2. The Mössbauer spectra of nanoparticles in magnetic field show a gradual increase of the hyperfine field parameter with increasing the nanoparticle size as a result of decreasing the relaxation rate. The S25 sample, however, demonstrates different behavior. In this case, the magnetic hyperfine field is considerably lower than for S20 sample. These effects together with the asymmetry on the right side of the S25 spectrum are signs of the additional ferrous six-line component. The correct analysis of these spectra demands generalization of the ferrimagnetic model temperature-dependent spectra to the case of an external magnetic field which will be shown in next studies.

Spectral parameters obtained from numerical fitting of the experimental spectra are shown in Table 1. The *KV* parameter of all samples was determined from the numerical fitting of the experimental spectra. The *KV* is connected with Néel's formula for the relaxation of the magnetization vector of the superparamagnetic particle. It is proportional to the barrier height, which the magnetization vector has to overcome in order to change its orientation to the opposite one. The barrier height is weakly dependent on the particle size. The samples S10 and S5 show approximately the same barrier height *KV* as the samples S15 and S20. The height of the barrier of sample S25 is less than that of S20, indicating a reduction in the strength of the dipole interactions. For comparison, the *KV* parameters were calculated by a second method, as multiplication of the anisotropy energy density with the volume of a single nanoparticle obtained from X-ray diffraction data (Table 2). In this case, the height of Néel's barrier strongly depends on the size of the single nanoparticle d_{XRD}. With increasing size d_{XRD}, parameter *KV* increases rapidly and reaches 2800 K for the sample S25.

4. Discussion

The X-Ray diffraction and Mössbauer measurements indicated the presence of an additional phase in the S25 sample. For Mössbauer spectra, the phase exhibits as an intense singlet for room temperature spectra (Fig. 3b). The isomer shift of this singlet is about 1.1 mm/s. The most probable candidate having the same isomer shift is ferrous iron FeO [22,23]. Fig. 4 shows the Mössbauer spectrum of FeO component synthesized in work [16]. This spectrum has almost the identical line shape and spectral parameters as the singlet component. In addition, the FeO component impacts on magnetic properties. The XRD pattern of the FeO component is only slightly different from the Fe_3O_4 one because of the similar crystal configuration of the two components [24]. The superposition of the two closely located diffraction peaks leads to the formation of an effectively broadened diffraction peak and consequently reduces the d_{XRD} parameter for S25. The magnetization curve for the S25 sample together with superparamagnetic component, which exists in the curves of the other samples, contains a paramagnetic component, which is proportional to a magnetic field magnitude. At low fields, the magnetization field dependence for S25 is lower than for S20. At higher fields, when growth of the superparamagnetic component decreases, the paramagnetic factor

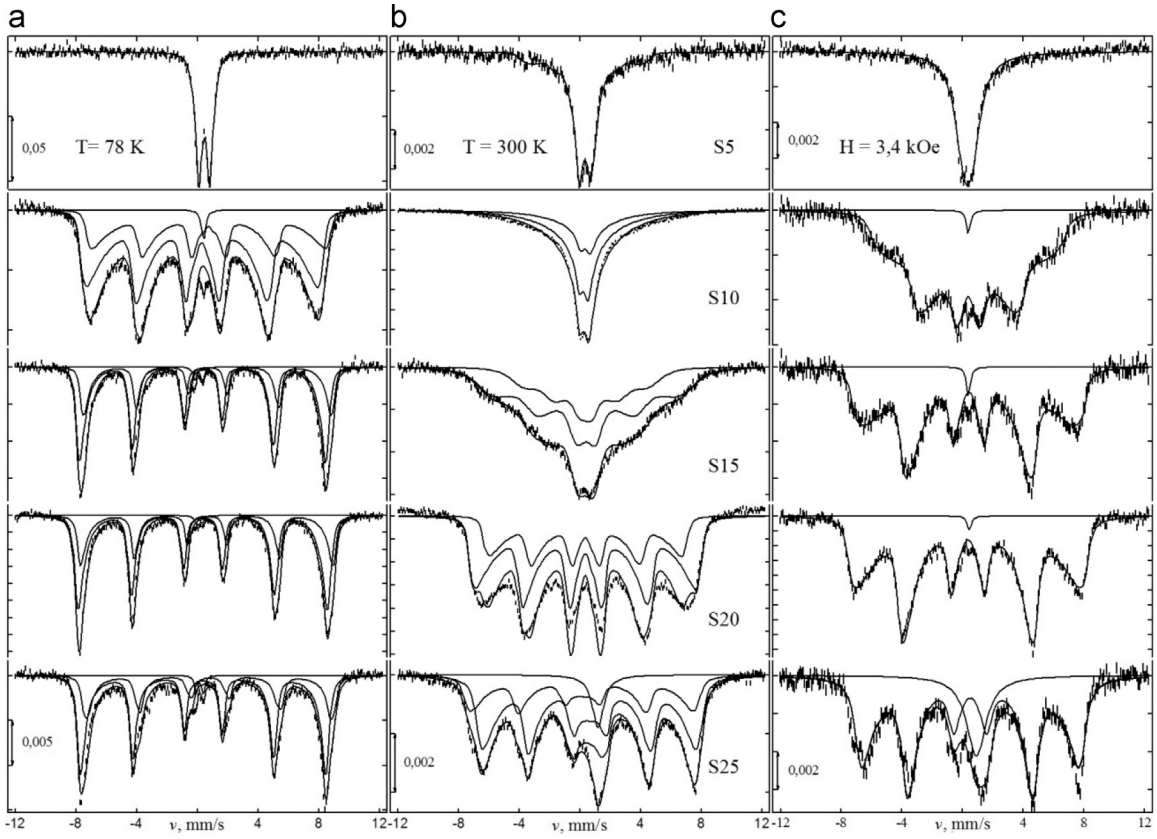

Fig. 3. Group of ^{57}Fe Mössbauer spectra, collected at 78 K (a), 300 K (b) and in the presence of a magnetic field with magnitude 3.4 kOe at 300 K (c) for the S5–S25.

Table 2
Parameters of the S10–S25 samples obtained from magnetization and magnetic field Mössbauer measurements. H_c=2 K/M_0-critical field, M_0-uniform saturation magnetization.

H_c, kOe	3.1 (2)	2.7 (1)	2.1 (1)	4.1 (2)
M_0, emu/g	5.5 (1)	17.0 (2)	20.3 (3)	25.0 (4)
$K_{magn} \times V_{XRD}$, K	210 (30)	1299 (200)	2800 (300)	2600 (300)

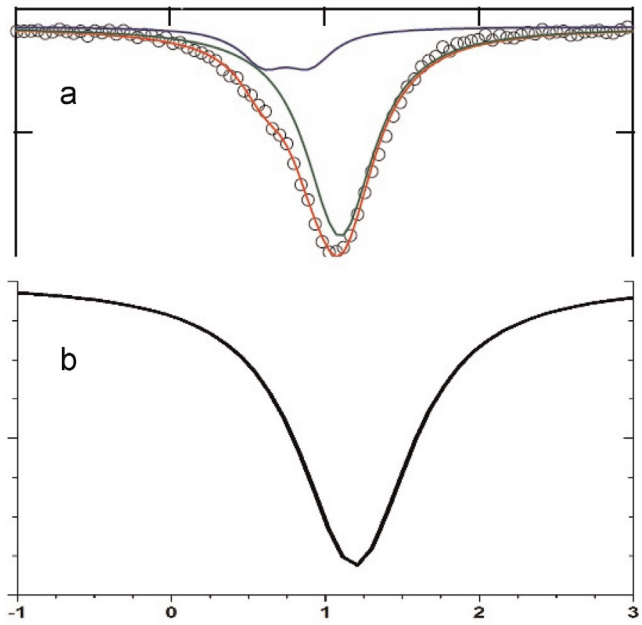

Fig. 4. (a) Mössbauer spectrum of FeO powder collected at 300 K. Taken from [16]. (b) Singlet component of the S25 300 K spectrum.

becomes significant and magnetization of the S25 sample exceeds magnetization of the S20 sample.

The Néel's height barriers for the samples S5 and S10 are approximately the same and equal 200 K. In addition, the spectrum of these samples at room temperature is a doublet, which indicates that the relaxation rates of the magnetization vectors of these samples went beyond the Larmor frequency of the nuclear spin precession. The samples of S15 and S20 at 78 K have a similar Néel's barrier height, which leads to almost identical spectral shape lines. However, the picture dramatically changes at 300 K. In the S15 spectrum a collapse of the hyperfine structure takes place, indicating a decrease in the size of the cluster of nanoparticles due to thermal disordering. For the S25 sample at 300 K *KV* is 540 K which is located between the barrier heights for the samples S15 and S20. This effect is caused by the superposition of the two factors: although the average size of the magnetic core for the S25 sample is more than that for the S15 sample, an additional paramagnetic surface phase weakens the strength of the dipole interactions, which results in decreasing *KV*. The *KV* parameter calculated as the direct multiplication ($K_{magn} \times V_{XRD}$) differs significantly from the *KV* parameter obtained from the Mössbauer spectra. The barrier is mainly determined by the size d_{XRD} and ignores the strength of the dipole interactions.

5. Conclusions

The present study has shown that in magnetite nanoparticles in the range 10–25 nm a ferromagnetic relaxation mechanism takes place in the absence of external magnetic field. The nanoparticle sizes estimated from TEM and X-ray diffraction did not correlate with nanoparticle magnetic properties. The main reason is that results of both of these methods can be influenced by additional

surface phases with magnetic responses different from the nanoparticle magnetic core. Mössbauer spectroscopy can be considered to be the most adequate method for describing the magnetic nanoparticle dynamics. The height of Néel's barrier *KV* directly estimated from Mössbauer data can be considered as a measure of the effective size of the cluster of the magnetic properties. Two methods for calculation of Néel's barrier height *KV* were considered: the direct calculation from an analysis of Mössbauer spectra and the separate calculation of the anisotropy constant and volume from magnetization and XRD data. The comparison of these methods demonstrated that the most reliable method is direct calculation of KV from an analysis of Mössbauer spectra.

Acknowledgment

This work is supported in part by the Russian Science Foundation under Grant 14-15-01096.

References

[1] M.P. Nikitin, R.R. Gabbasov, V.M. Cherepanov, M.A. Chuev, M.A. Polikarpov, V. Y. Panchenko, S.M. Deyev, AIP Conf. Proc. 1311 (2010) 401–407.
[2] R.R. Gabbasov, V.M. Cherepanov, M.A. Chuev, M.A. Polikarpov, M.P. Nikitin, S. M. Deyev, V.Y. Panchenko., IEEE Trans. Magn. 49 (2013) 394–397.
[3] D. Polikarpov, V. Cherepanov, M. Chuev, R. Gabbasov, I. Mischenko, M. Nikitin, Y. Vereshagin, A. Yurenia, V. Panchenko, Hyp. Int. 226 (2014) 421–430.
[4] Q. Pankhurst, et al., Applications of magnetic nanoparticles in biomedicine, J. Phys. D Appl. Phys. 36 (13) (2003) 167–181.
[5] O. Veiseh, J.W. Gunn, M. Zhang, Design and fabrication of magnetic nanoparticles for targeted drug delivery and imaging, Adv. Drug Deliv. Rev. 62 (3) (2010) 284–304.
[6] H. Khurshid, S.H. Kim, et al., Development of heparin-coated magnetic nanoparticles for targeted drug delivery applications, J. Appl. Phys. 105 (7) (2009) 308–315.
[7] R. Hergt, S. Dutz, R. Muller, M. Zeisberger, Magnetic particle hyperthermia: nanoparticle magnetism and materials development for cancer therapy, J. Phys. Condens. Matter 18 (38) (2006) 2919–2934.
[8] R.R. Gabbasov, M.A. Polikarpov, V.M. Cherepanov, M.A. Chuev, V.Y. Panchenko., Hyp. Int. 206 (2012) 71–74.
[9] S. Mørup, D.E. Madsen, C. Frandsen, C.R.H. Bahl, M.F. Hansen, J. Phys.: Condens. Matter 19 (2007) 213202.
[10] S. Mørup, M.F. Hansen, C. Frandsen, Compr. Nanosci. Technol. 1 (2011) 437–491.
[11] M.A. Chuev, JETP 114 (4) (2012) 609–630.
[12] J.S. Salazar, L. Perez, O.D. Abril, L.T. Phuoc, D. Ihiawakrim, M. Vazquez, G. Pourroy, Chem. Mater. 23 (2011) 1379–1386.
[13] T.J. Daou, J.-M. Greneche, S.-J. Lee, S. Lee, C. Lefevre, S. Colin, G. Pourroy, J. Phys. Chem. C 114 (2010) 8794–8799.
[14] M.D. Carvalho, F. Henriques, L.P. Ferreira, M. Godinho, M.M. Cruz, J. Solid State Chem. 201 (2013) 144–152.
[15] R.R. Gabbasov, V.M. Cherepanov, M.A. Polikarpov, V.Y. Panchenko., Hyp. Int. 226 (2014) 383–387.
⟨http://www.oceannanotech.com⟩ ⟨http://www.oceannanotech.com⟩.
[17] H. Duan, M. Kuang, X. Wang, Y.A. Wang, H. Mao, S. Nie., J. Phys. Chem. C 112 (22) (2008) 8127–8131.
[18] W.W. Yu, J.C. Falkner, C.T. Yavuz, V.L. Colvin, Chem. Commun. (2004) 2306–2307.
[19] M.A. Chuev, J. Exp. Theor. Phys. 108 (2009) 249–259.
[20] M.A. Chuev, J. Exp. Theor. Phys. Lett 98 (8) (2013) 465–470.
[21] M.A. Chuev, J. Exp. Theor. Phys. Lett 99 (5) (2014) 278–282.
[22] T. Yoshikawa, Y. Kanke, H. Yanagihara, E. Kita, Y. Tsunoda, K. Siratori, K. Kohn, Hyp. Int. 205 (2012) 135–138.
[23] L. Di Felice, C. Courson, D. Niznansky, P.U. Foscolo, A. Kiennemann, Energy Fuels 24 (2010) 4034–4045.
[24] T.J. Daou, G. Pourroy, S. Begin-Colin, J.M. Greneche, C. Ulhaq-Bouillet, P. Legare, P. Bernhardt, C. Leuvrey, G. Rogez, Chem. Mater. 18 (2006) 4399–4404.